ARTICLES
https://doi.org/10.1038/s42256-019-0091-7
nature machine intelligence

Fully portable and wireless universal brain–machine interfaces enabled by flexible scalp electronics and deep learning algorithm

Musa Mahmood[1], Deogratias Mzurikwao[2], Yun-Soung Kim[1], Yongkuk Lee[3], Saswat Mishra[1], Robert Herbert[1], Audrey Duarte[4], Chee Siang Ang[2] and Woon-Hong Yeo[1,5,6*]

Variation in human brains creates difficulty in implementing electroencephalography into universal brain–machine interfaces. Conventional electroencephalography systems typically suffer from motion artefacts, extensive preparation time and bulky equipment, while existing electroencephalography classification methods require training on a per-subject or per-session basis. Here, we introduce a fully portable, wireless, flexible scalp electronic system, incorporating a set of dry electrodes and a flexible membrane circuit. Time-domain analysis using convolutional neural networks allows for accurate, real-time classification of steady-state visually evoked potentials in the occipital lobe. Compared to commercial systems, the flexible electronics show the improved performance in detection of evoked potentials due to significant reduction of noise and electromagnetic interference. The two-channel scalp electronic system achieves a high information transfer rate (122.1 ± 3.53 bits per minute) with six human subjects, allowing for wireless, real-time, universal electroencephalography classification for an electric wheelchair, a motorized vehicle and a keyboard-less presentation.

Compared to other methods for electrophysiological monitoring of the brain, modern electroencephalography (EEG) systems provide non-invasive monitoring of brain electrical activity with fine temporal resolution, ease of use and relatively low cost. Thus, EEG-based brain–machine interfaces (BMIs) have been widely used for rehabilitation through control of prosthetic systems or substitutive control[1–4]. BMIs can restore freedom of movement and improve quality of life for chronic stroke survivors with locked-in syndrome or people with amyotrophic lateral sclerosis or another severe motor disability[5–8]. The capture and classification of steady-state visually evoked potentials (SSVEP) is one potential strategy for therapeutic BMIs[9–12]. For this type of interface, the subject is requested to focus on flickering stimuli (computer screens or external light sources), while an EEG system captures brain electrical activity from specific locations on the scalp[13–15]. These stimuli elicit frequency-dependent brain activity, and therefore arrays of stimuli may be used as an interface for subjects to gaze between for control over some target[16–19]. Conventional EEG set-ups for SSVEP acquisition use a hair-cap or crown-like set-up, with many metal electrodes, up to 256 channels[20–22]. These systems are bulky and heavy, with uncomfortable, rigid metal scalp electrodes. These electrodes are often coupled with conductive gels or pastes to adequately capture the signal. Variances in scalp hair thickness and density cause variations in impedance between electrode locations[23]. Gel-based electrodes take considerable time to set up and require regular maintenance[24,25]. Furthermore, water-based gels evaporate over time, causing decay in skin–electrode contact impedance[15]. Recent research in EEG design displays a trend towards wearable and wireless EEG devices[26]. These are preferable for day-to-day mobile EEG monitoring, with short set-up times and excellent long-term performance provided adequate skin preparation with optimal amplifier, shielding and electrode configurations[25,27]. New systems featuring dry electrodes perform as well as, if not better than, conventional systems, establishing strong groundwork towards a transition to dry-electrode-based electrophysiological systems[15,27,28]. There is also an argument for the use of lightweight sensors and shorter leads to prevent dragging or movement artefacts that may occur with massy cap EEG systems[29]. However, the available mobile EEG systems[30–33] are still quite bulky and use rigid electronic and structural components with a large number of electrodes, which are not comfortable for daily use and real-world applications. Here, we introduce an example of a fully portable, wireless, flexible, skin-like hybrid scalp electronic system (referred to as 'SKINTRONICS') that includes a low-profile, flexible circuit, an ultrathin aerosol-jet-printed skin electrode and three flexible conductive polymer electrodes for mounting on the hairy scalp (occipital lobe). The primary novelty is in the development of a fully integrated packaging of high-resolution EEG monitoring sensors and circuits within a miniaturized skin-conformal system. This soft electronic system is capable of improved EEG performance for idle, seated subjects owing to its simplicity of design and compactness, and its absence of motion artefacts caused by long wires and electrode movements, typically found in other EEG systems. SKINTRONICS offers maximal comfort and minimal set-up time, requiring only two channels on the occipital lobe to measure SSVEPs with competitive information transfer rates (ITRs). We demonstrate a capability to train deep

[1]George W. Woodruff School of Mechanical Engineering, Institute for Electronics and Nanotechnology, Georgia Institute of Technology, Atlanta, GA, USA. [2]School of Engineering and Digital Arts, University of Kent, Canterbury, UK. [3]Department of Biomedical Engineering, Wichita State University, Wichita, KS, USA. [4]School of Psychology, College of Sciences, Georgia Institute of Technology, Atlanta, GA, USA. [5]Wallace H. Coulter Department of Biomedical Engineering, Parker H. Petit Institute for Bioengineering and Biosciences, Georgia Institute of Technology, Atlanta, GA, USA. [6]Neural Engineering Center, Center for Flexible and Wearable Electronics Advanced Research, Institute for Materials, Institute for Robotics and Intelligent Machines, Georgia Institute of Technology, Atlanta, GA, USA. *e-mail: whyeo@gatech.edu

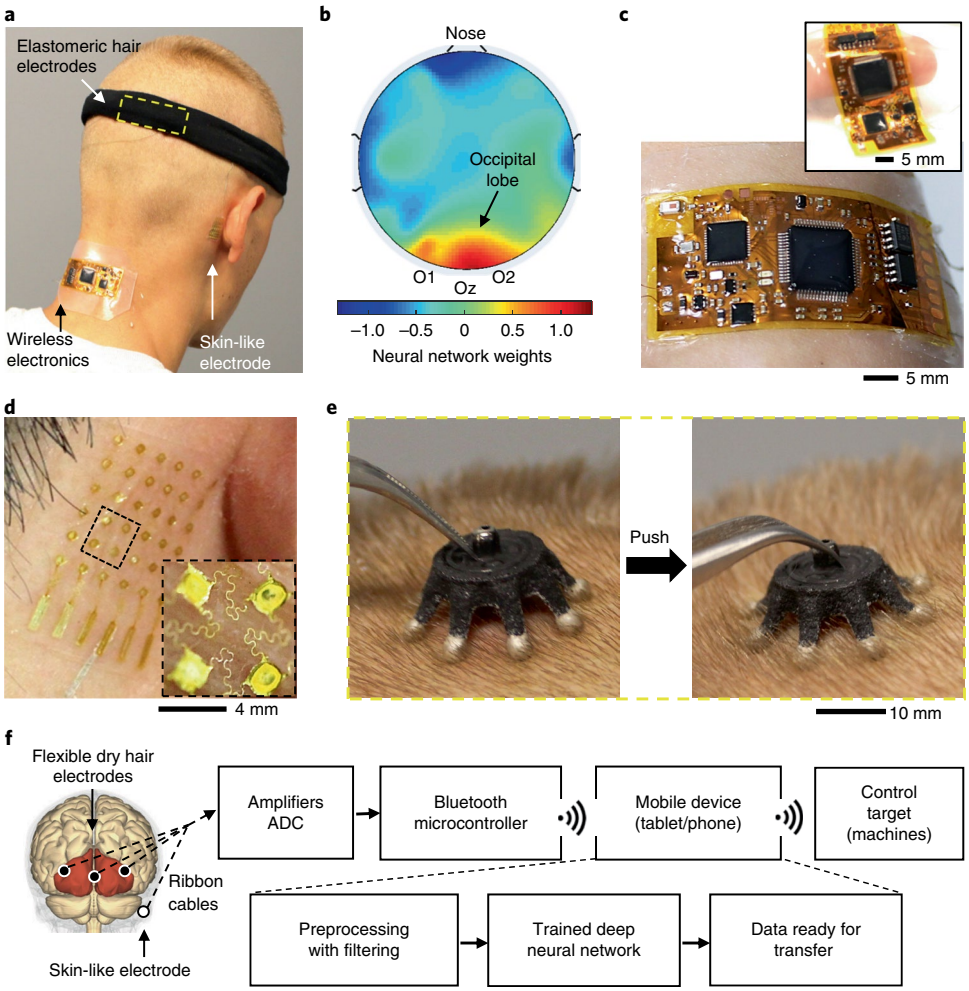

Fig. 1 | Overview of the system architecture featuring fully portable and wireless scalp electronics. a, A photo of a subject who has flexible wireless electronics (SKINTRONICS) conformed to the back of the neck with dry hair electrodes under a fabric headband and a membrane electrode on the mastoid, connected via thin-film cables. **b**, A neural network-based topographical map that indicates EEG signal amplitudes. **c**, A photo capturing the ultrathin, flexible wireless electronics on skin, with an inset demonstrating device flexibility while handling. **d**, An aerosol-jet-printed stretchable, skin-like electrode with an open-mesh structure (inset). **e**, Images showing gentle splaying of the conductive flexible elastomer legs of a dry hair electrode when slight downward pressure is applied, allowing the legs to separate the hair and the Ag/AgCl-tipped legs to achieve good contact with the scalp. **f**, An illustration (left) showing the electrode positions on a posterior view of the brain and the occipital lobe (highlighted in red) and a flow chart (right) describing the entire process of EEG-enabled BMIs. ADC, analog-to-digital converter.

convolutional neural networks (CNNs) offline and integrate them into wireless mobile devices for real-time, universal EEG classification. Furthermore, optimization of the system set-up and classification model enables a highly competitive ITR[34] (122.1 ± 3.53 bits per minute) using only two channels, far fewer than most other systems achieving similar values. Applications for this system, including a powered wheelchair interface designed for subjects with locked-in syndrome or another motor disability, are demonstrated. With ever-improving mobile processing power, the combination of many-channel SKINTRONICS with an integrated universal BMI demonstrates possible implications for the use in portable EEG-based neuroprosthetics, real-time diagnosis of neurological disorders or neuro-assisted learning (classroom support).

Results

Device architecture and skin integration of a scalp electronic system. Figure 1 shows an overview of the wireless, portable scalp electronics for a SSVEP-based BMI. The photo in Fig. 1a captures the design concept of the flexible electronic system that minimizes the contact area (only two channels) on the scalp for a comfortable, dry EEG recording. The fully flexible, wearable system enables real-time long-range wireless data acquisition and accurate classification of SSVEPs with a high ITR from only two recording channels. Owing to the extreme mechanical compliance and small form factor, SKINTRONICS exhibits a significant reduction of noise and electromagnetic interference, compared to the existing portable EEG systems with rigid electronic components[33,35–37]. Furthermore, the use of conformal electronic components allows for easy wearability on the back of the neck or other bare skin locations. This soft system allows for long-term wear versus other rigid devices with heavy plastic enclosures that have to be clipped-on or worn in an uncomfortable manner. Overall, the integrated electronics on the scalp, in conjunction with a deep learning algorithm, demonstrates the feasibility for a real-time, highly accurate in vivo BMI via SSVEP data from two channels. Figure 1b shows the optimal electrode locations as determined by a deep CNN analysis of a 32-channel EEG recording of SSVEP data (details in Methods; Supplementary Fig. 1 and Supplementary Section 1). The electrode positions in Fig. 1b (O1, Oz and O2) were determined in preliminary tests to have consistently high signal-to-noise ratios (SNRs) across all tested subjects.

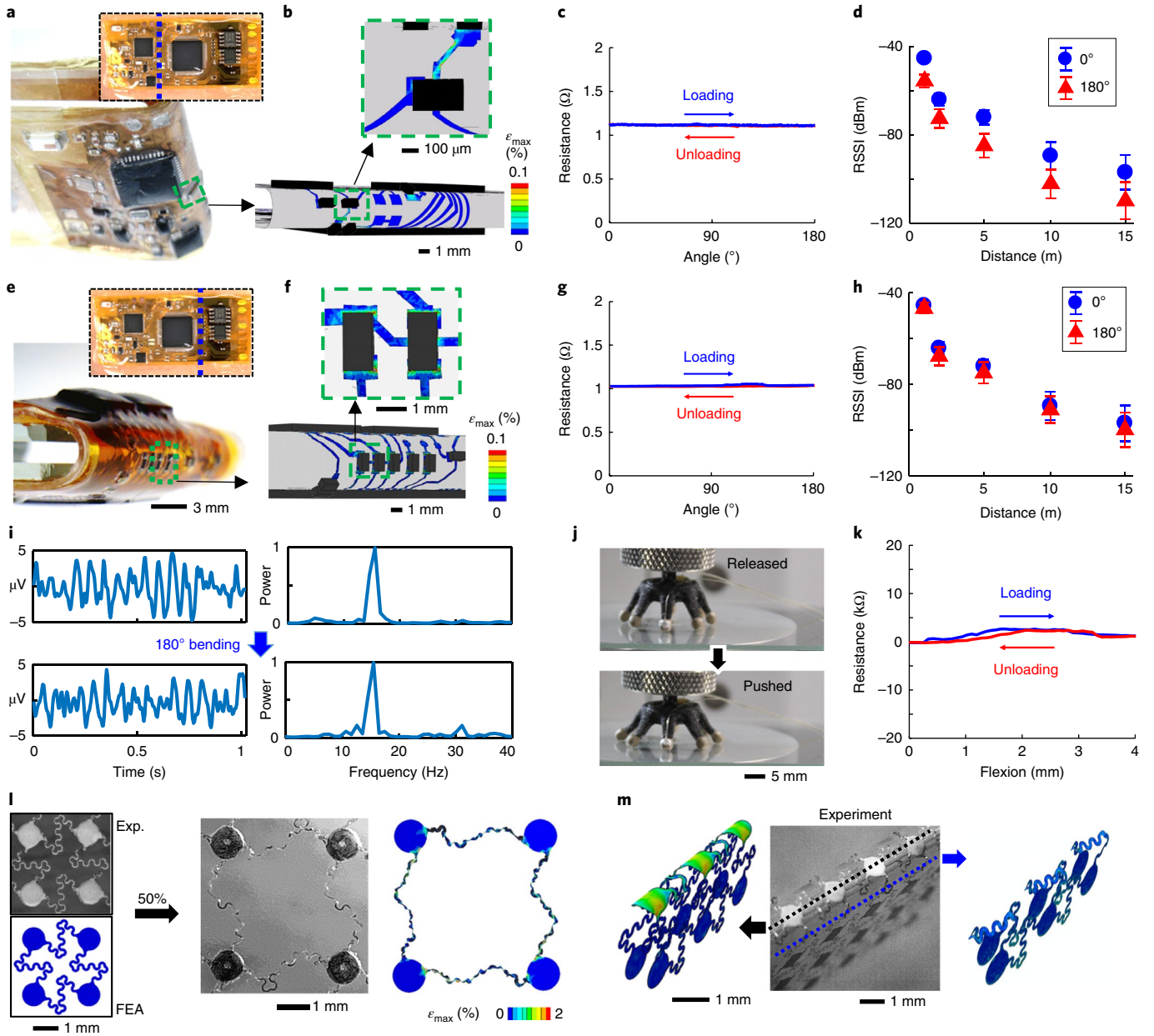

Fig. 2 | Mechanical flexibility and stretchability of the scalp electronics. a, A photo of the electronics bent at the first location along the vertical axis, as shown in the inset photo, demonstrating 180° bending (radius of curvature: 1.3 mm). **b**, FEA of the fine mesh structure simulating 180° bending with the same radius resulting in minimal strain at the interconnects (scale bar: maximum principal strain). **c**, Measurement of electrical resistance for the device under cyclic bending between 0 and 180°, showing negligible changes in resistance. **d**, RSSI response at 0° and 180° with different distances up to 15 m ($n = 3$ samples, error bars = standard error). **e**, The device bent at the second location along the vertical axis, as shown in the inset photo, between the analog-to-digital converter and the amplifiers (radius of curvature: 1.3 mm). **f**, FEA of the flexible structure simulating 180° bending with minimal strain (scale bar: maximum principal strain). **g**, Measurement of the cyclic bending effect on the device in **e**, by recording the change of electrical resistance. **h**, RSSI response up to 15 m at 0° and 180° bending ($n = 3$ samples, error bars = standard error). **i**, 15.2 Hz SSVEP data recorded without (top) and with 180° bending (bottom). **j**, A hair-based elastomer electrode under compression. **k**, Corresponding load and unload curves showing a negligible peak change in resistance over a 6 s cycle. **l**, A subunit of a skin-mounted electrode under 100% stretching in experiment and FEA, showing no mechanical failure. **m**, A 180° bending test of the electrode, showing less than 2% strain in FEA and no mechanical defects in experimental observation.

Deep CNN analysis is used to isolate the best electrodes from a larger cluster of electrodes, as it does not require prior knowledge of the signal type. This method is useful when the signal's features are difficult to decompose by conventional methods (for example, power spectrum analysis). The miniaturized, multi-channel flexible electronic system (Fig. 1c), encapsulated in a soft elastomeric membrane, was fabricated by using a combination of microfabrication techniques[38], material transfer printing[38] and hard–soft component integration[39] (details in Methods; Supplementary Figs. 2 and 3). This manufacturing process allows the production of a skin-conformal, unobtrusive and comfortable EEG device. The EEG recording set-up for two channels (O1–Oz and O2–Oz) incorporates an aerosol-jet-printed skin-like electrode (Fig. 1d) and elastomeric hair electrodes (Fig. 1e). The highly conformal membrane electrode is placed at the right mastoid to serve as a driven ground. We utilize a set of dry, flexible elastomeric electrodes (Cognionics) that make

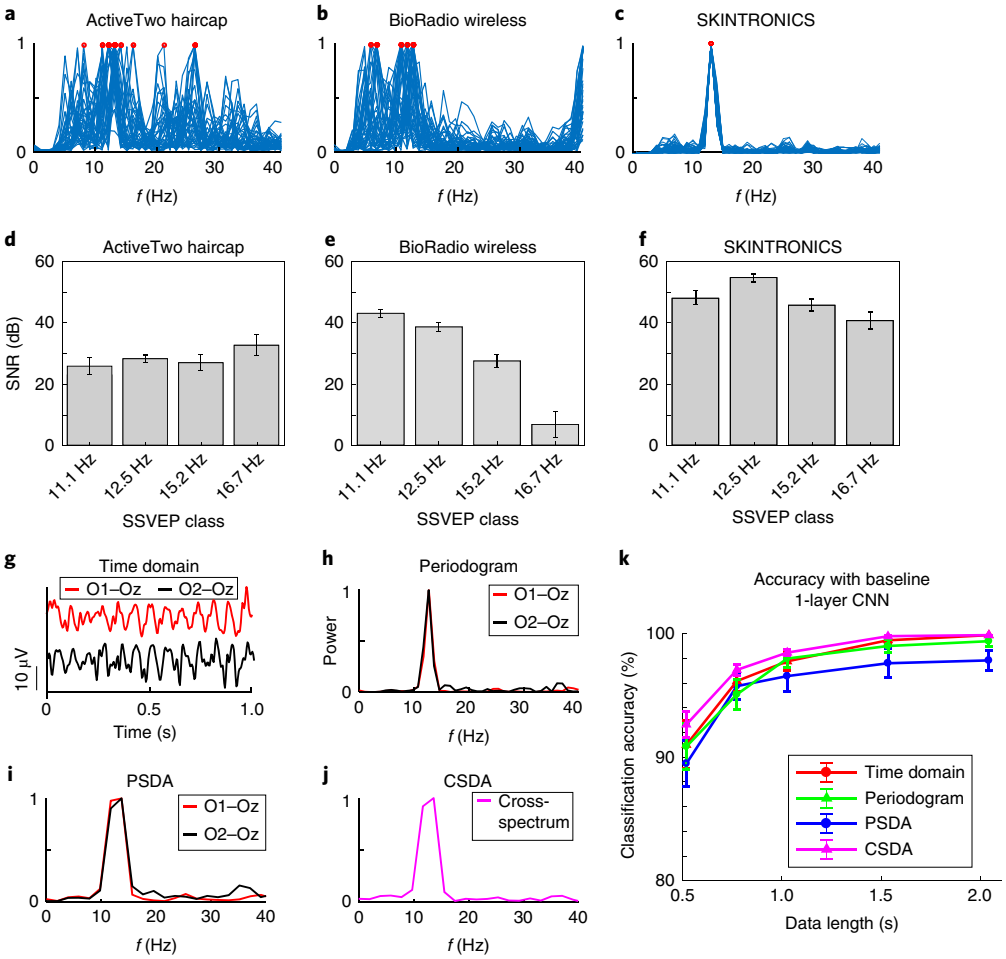

Fig. 3 | Comparison of device signal quality and classification accuracy. Three data sets for a conventional EEG system (ActiveTwo; first column), a bulky clip-on wireless system (BioRadio; second column) and our two-channel SKINTRONICS system (third column). **a**–**c**, Periodograms of 50 samples from 12.5 Hz SSVEP signals overlaid over each other, with peaks highlighted with red circles; this comparison illustrates our device's ability to precisely target and capture SSVEP signals without excessive noise. **d**–**f**, Average SNR with four SSVEP classes, across all six tested subjects. The error bars represent the standard error of the mean ($n = 60$ recordings; 6 subjects, 10 recordings each). **g**, Two-channel SSVEP data at 12.5 Hz in the time domain. **h**, Further preprocessing in the form of frequency analysis including a single-window periodogram. **i**, A Welch PSDA overlapping periodogram. **j**, CSDA of both channels. Note that the cross-spectral input includes the normal Welch power spectrum, resulting in three features. **k**, Comparison of the classification accuracy between four preprocessing methods, shown in **g**–**j**. The points on the graph are the mean accuracies from 36 trials from all 6 test subjects. The error bars represent the standard error of the mean ($n = 36$ trials).

intimate contact to the hairy region, resulting in long-term EEG recording[40]. With adequate skin preparation, the conformal contact provided by these electrodes allows for superior skin impedance (less than 20 kΩ), and therefore lower noise in signal recording and transmission. In addition, there are only three scalp electrodes, effectively secured by using a single headband, which allows the electrodes to splay their legs, separating and moving hair, to make effective contact with the scalp as demonstrated in Fig. 1e. The flow chart in Fig. 1f shows a high-level overview of data collection, processing, wireless transfer and machine control (details of the EEG circuit are provided in Supplementary Fig. 4).

Quantitative study of system mechanics and reliability. To build a portable, wearable scalp electronics, intimate skin integration is critical while allowing the wearer to conduct everyday activity. The device must also maintain its ability to acquire high-fidelity EEG signals along with wireless transmission of data while under bending. In this work, we subject the electronics to 180° bending up to 1.3 mm in radius of curvature, well beyond the expected bending during skin deformation on the back of the neck. Similar mechanical tests are performed on the hair electrode and skin-like electrode to ensure long-term mechanical stability on the skin application. Computational finite element analysis (FEA) was used to design the electronic circuit and wearable electrode, which provided an optimal design to endure continuous mechanical deformation. Afterwards, a set of experiments demonstrated the mechanical reliability of the SKINTRONICS (Fig. 2), including microscope investigation, resistance measurement and received signal strength indication (RSSI). Details of the computational and experimental study procedures appear in the Methods. The flexible electronic circuit shows great mechanical stability on cyclic bending along the vertical axis for the first location (Fig. 2a–d) and second location (Fig. 2e–h). Details of the bending points are summarized in Supplementary Fig. 5a. With a complete folding of the device at a bending radius of 1.3 mm (Fig. 2a), the device shows no adverse effects, as supported by the FEA result (Fig. 2b) with negligible change in the maximum principal strain (<0.1 %). The change of electrical resistance of the interconnects in Fig. 2a is measured during the cyclic loading and unloading process (Fig. 2c), which also shows consistent resistance with the maximum change of 0.06 Ω.

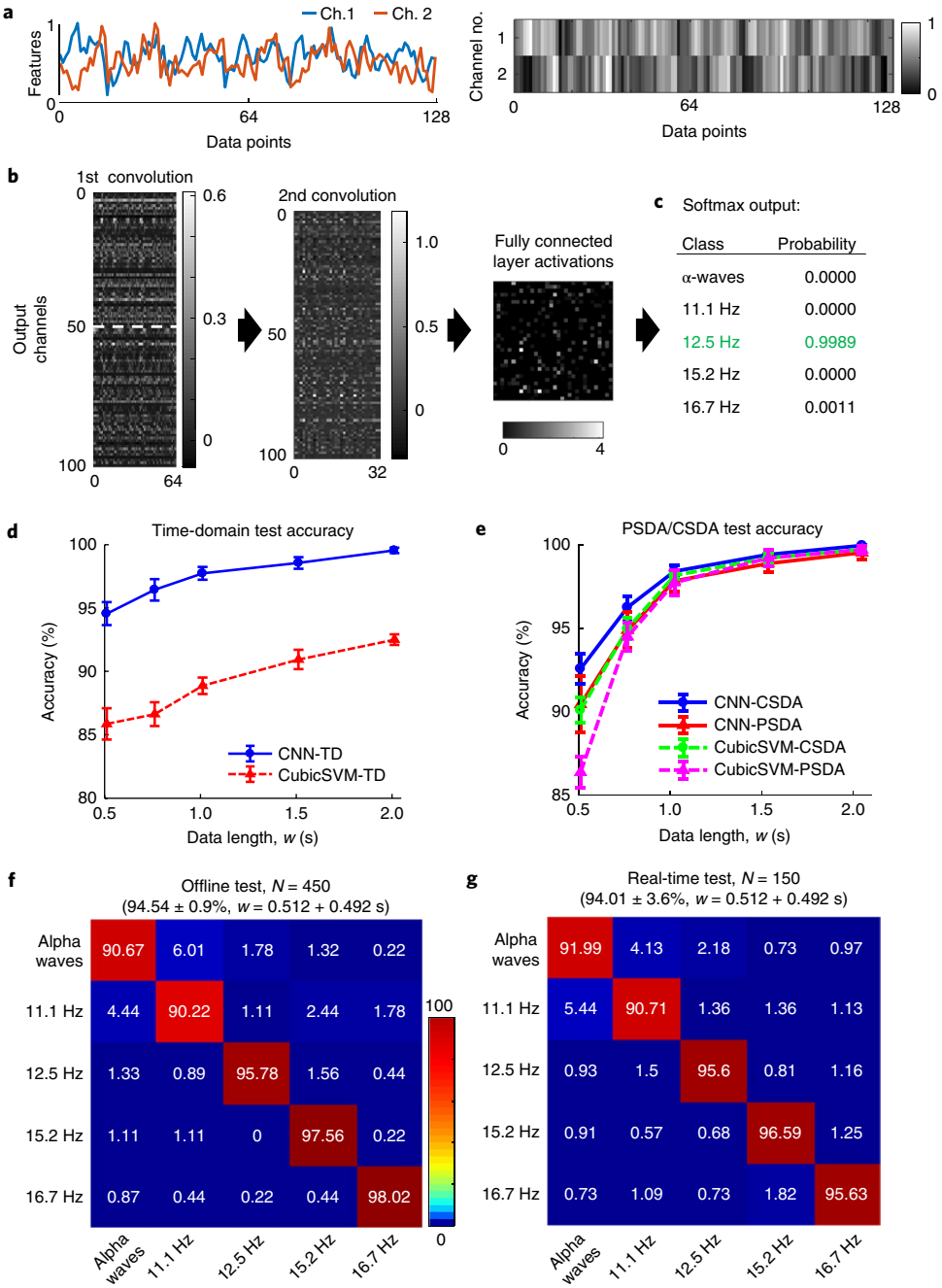

Fig. 4 | EEG classification with CNNs. a, High-pass-filtered raw EEG data in the time domain with features linearly rescaled between 0 and 1, labelled as SSVEP class '12.5 Hz', along with a representative greyscale image. **b**, A greyscale representation of the output weights in the two layers of CNNs as well as in the fully connected layer using the 2-CNN model for the time-domain data. **c**, A table of softmax class outputs, indicating a correct choice with 99.89% probability. **d**, CNN and SVM classification test accuracy using time-domain data and cross-validating across all subjects ($n = 6$ subjects, 450 samples, error bars = standard error). **e**, CNN and SVM test accuracy on frequency-domain data, cross-validating across all subjects, with window lengths from 0.512 to 2.048 s. The displayed results are from the strongest SVM of the four tested (cubic kernel) ($n = 6$ subjects, 450 samples, error bars = standard error). **f**, A confusion matrix representing the results from the offline accuracy test of time-domain data of data window length $w = 0.512$ s, with an overall accuracy of 94.54% ($n = 2{,}700$ samples; 6 subjects, 450 samples each). **g**, A confusion matrix representing results from the real-time accuracy test of time-domain data of length $w = 0.512$ s, with an overall accuracy of 94.01% ($n = 2{,}700$ samples; 6 subjects, 450 samples each).

Additionally, the RSSI measurement monitors the wireless signal quality under 180° bending up to 15 m (Fig. 2d), showing that the device maintains connectivity at distances over 10 m. Details of the mechanical bending configuration are shown in Supplementary Fig. 5b. Another location of the electronics shows 180° bending with a radius of 1.6 mm (Fig. 2e). The corresponding FEA in Fig. 2f shows similar results to those for the first location, and the interconnects are intact after bending. Figure 2g shows the resistance measurements at this location where the maximum change in resistance is 0.09 Ω, indicating the stability of the interconnects during cyclic bending. The RSSI investigation (Fig. 2h) validates the device's functionality with distances up to 15 m. The resistance

Table 1 | Comparison of ITRs between the SKINTRONICS system and reported values

	Year	Accuracy (%)	Length (s)	Number of classes	Number of channels	ITR (bits per minute)
This work (SKINTRONICS)	2019	94.54	0.94	5	2	122.1 ± 3.53
Nakanishi et al.[30]	2018	89.83	0.8	40	9	325.33 ± 38.17
Chen et al.[44]	2015	91.09	1	40	9	270.0 ± 61.8
Bevilacqua et al.[59]	2014	95.61	2	3	4	38.44[a]
Kwak et al.[31]	2017	99.19	2	5	8	67.13[a]
Volosyak et al.[60]	2011	96.79	2	5	8	61.70 ± 32.68
Lin et al.[18]	2007	73.00	1.5	9	8	60.74[a]
Bin et al.[20]	2009	95.30	2	5	8	58.6 ± 9.6
Wang et al.[14]	2010	97.20	3.08	16	10	72.2

[a]Values calculated from the reported data.

measurements at each location after 100 bending cycles are shown in Supplementary Fig. 5c, showing a slight increase in resistance, from 1.19 to 1.51 Ω at location 1, and from 1.08 to 1.38 Ω at location 2. Furthermore, recorded SSVEP data (stimulus at 15.2 Hz) that compares the effect of cyclic bending of the electronics (Fig. 2i) shows negligible change in the signal quality. The elastomeric hair-based electrodes underwent cyclic compression testing while monitoring resistance from the connector to a single leg of the electrode. The method is briefly described in Supplementary Section 4, with the set-up shown in Supplementary Fig. 6. A maximum compression of 2 mm, followed by release over a 6 s period (Fig. 2j), was repeated for 1,000 cycles, simulating the maximum compression exhibited during EEG recording. During a single cycle of compression, the peak change in resistance was only 4.1 kΩ (Fig. 2k). Even with 1,000 cycles, the uncompressed resistance changed a total of 4.46 kΩ (less than 10% of the initial resistance; Supplementary Fig. 7). The conductive elastomeric electrodes showed excellent resilience to mechanical stress and were still capable of measuring EEG signals after the test was completed. These results are supported by a prior study that evaluated the robustness of these electrodes in a high-density multi-channel system[41]. For EEG recording, a skin-like silver electrode undergoes multimodal bending and stretching on mastoid due to time-dynamic movements with the ear. For bending tests, a set-up like the one used in Supplementary Fig. 5 for testing SKINTRONICS was used. Resistance change during bending was also measured, showing stability under complete folding at a small radius. The summary of the experimental and computational study in Fig. 2l,m validates the structural safety of the printed electrode, with over 50% biaxial strain and up to 180° bending at the radius of 250 μm (details in Supplementary Figs. 8 and 9). The FEA results show the maximum strain under 1% in any region of the electrode, while microscopic observation captures no fracture lines. This evidence, in addition to our prior studies evidencing long-term reliability[15,38,42] regarding skin-wearable electrodes, demonstrates the mechanical stability of the SKINTRONICS device and electrodes for extended human use.

Analysis of signal quality and classification accuracy. The new electronic system, SKINTRONICS, is benchmarked against two state-of-the-art EEG monitoring devices. The first is a 32-channel EEG system (ActiveTwo System, Biosemi), using water-based conductive gels (SignaGel, Parker Laboratories). The second is a wireless, portable system (BioRadio, Great Lakes NeuroTechnologies) that allows for eight channels in a referential montage. We demonstrate the functionality and performance of the SKINTRONICS system via the direct comparison with these commercial systems. The ActiveTwo 32-channel system uses Ag/AgCl active electrodes to represent the gold standard, benchtop EEG system, while the BioRadio represents a wireless, handheld EEG and uses dry, flexible elastomeric electrodes (Cognionics) as a control to compare the performance of the SKINTRONICS system. The detailed procedure for data acquisition is provided in the Methods. Figure 3 summarizes the comparison of SSVEPs captured using a single occipital lobe channel (O1–Oz), by three different systems. The side-by-side comparison of the 12.5 Hz SSVEP data captures the superior performance of the SKINRONICS system (Fig. 3a–c) with the consistent and overlapping peaks of 12.5 Hz from the first channel (O1–Oz). In these panels, periodograms from 50 consecutive 1 s sample windows with 128 ms overlap from a single subject are overlaid on a single graph to demonstrate the signal variance from each of the three devices. SNR analysis (Fig. 3d–f) for all six subjects was performed offline in a numerical program (MATLAB, MathWorks). The method used for calculating SNR is provided in the Methods. Among the three systems, the SKINTRONICS system shows the highest average SNR (46.6 ± 2.16 dB) from four SSVEP classes, measured with 6 human subjects. This shows that the SKINTRONICS SNR is a significant improvement over the conventional gel-based system (ActiveTwo; 16.94 ± 4.60 dB) and the portable wireless system with dry electrodes (BioRadio; 28.89 ± 2.28 dB). Figure 3g–k demonstrates each of four preprocessing and analysis methods with a 1.024 s segment of 12.5 Hz SSVEP data. Two-channel (O1–Oz and O2–Oz) time-domain data (Fig. 3g) are converted to a single-window periodogram (Fig. 3h), power spectral density analysis (PSDA; Fig. 3i) and cross-spectral density analysis (CSDA; Fig. 3j). The details of the PSDA and CSDA methods are shown in Supplementary Sections 6 and 7, respectively. The primary metric used to establish the efficacy of the EEG system is the ITR, calculated in bits per unit time, as shown in the Methods. To further quantify the SKINTRONICS performance, we conducted a canonical correlation analysis (CCA; details in Supplementary Section 5). Our system achieves an average accuracy of 89.6 ± 2.1% at the shortest data length of 0.512 s for 4 SSVEP classes over 6 human subjects (original datasets in Supplementary Fig. 10 and original accuracy of 7 SSVEP classes in Supplementary Fig. 11 with details in Methods). To improve on the classification accuracy achieved using CCA, we utilized support vector machines (SVMs) and CNNs[31]. Feature extraction and classification techniques are detailed in the Methods and Supplementary Fig. 12. The summary of the resulting accuracies from four datasets appears in Fig. 3k, which is based on one-layer CNN analysis (architecture provided in Supplementary Table 2). These preliminary results suggest that the basic network most effectively extracts features from CSDA and time-domain data.

Optimization of CNNs. One of the key study points of this work is to show the universal capability to classify SSVEPs from two channels on any subject. Therefore, sixfold cross-validation is performed on

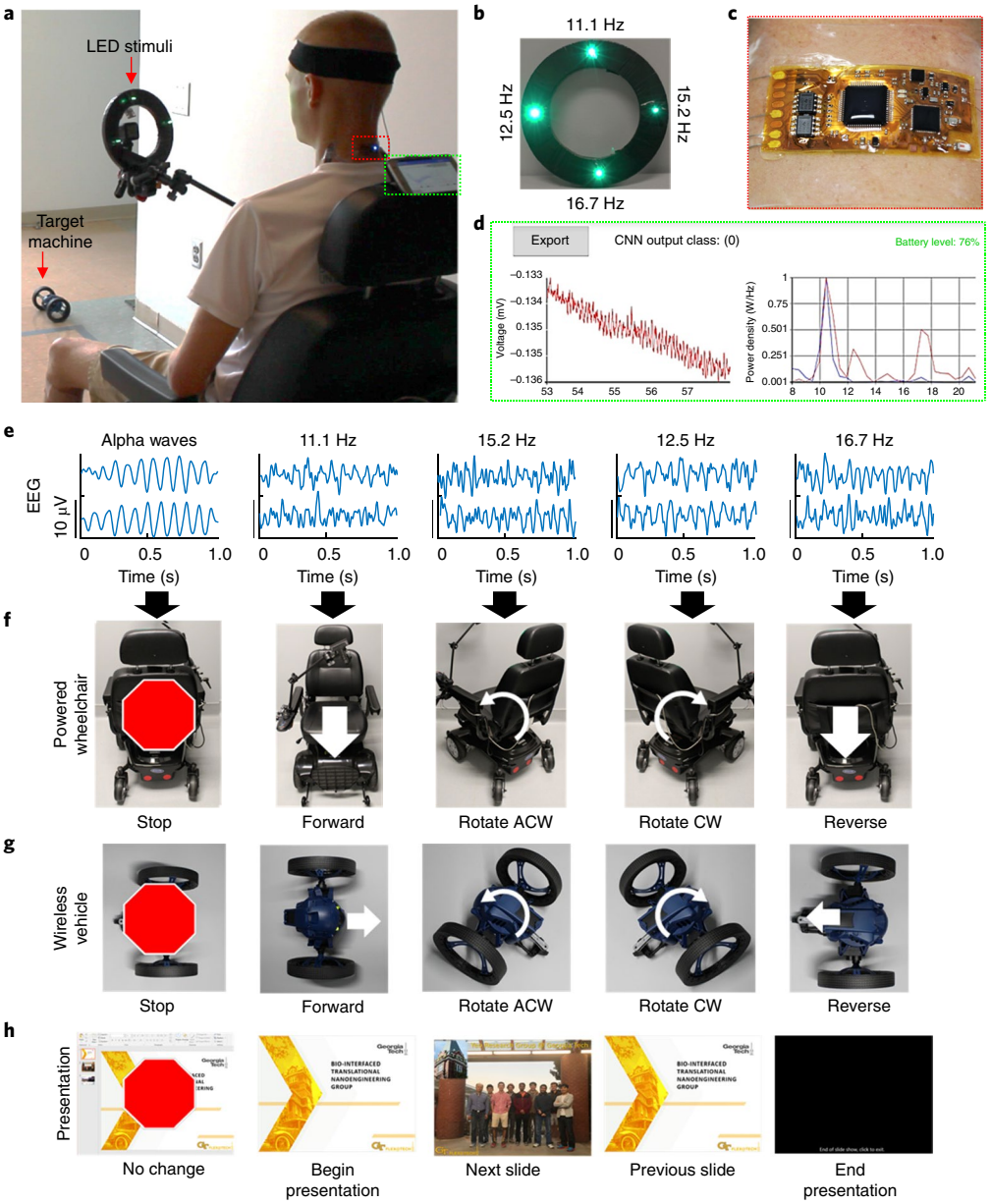

Fig. 5 | In vivo demonstration of the SKINTRONICS BMI with human subjects. a–c, A subject seated in a powered wheelchair (**a**) with the LED stimulus array (**b**) and the SKINTRONICS system secured and conforming to the back of the neck (**c**). **d**, The Android user interface during training and evaluation, showing time-domain data, the corresponding power spectrum and the output class. **e**, EEG data recorded at each state, labelled as alpha rhythms, 11.1 Hz, 15.2 Hz, 12.5 Hz and 16.7 Hz SSVEPs respectively. **f–h**, Three target machines to control via SSVEP signals, including a wireless electric wheelchair (**f**) with five classes (no action, forward, rotate anticlockwise (ACW), rotate clockwise (CW) and reverse), a wireless vehicle (**g**) with the same commands as the wheelchair and a PowerPoint presentation (**h**) with five-class actions (no action, begin presentation, next slide, previous slide and end presentation).

a subject-to-subject basis as described in the Methods. The experimental classes, along with procedures for preparing training and test data, are also provided. Here, CNNs are used to classify signals from the five classes. With shared weights, CNNs can detect features on either channel at any location, while keeping the size of the network relatively small[43]. For the most basic one-layer CNN, a grid-search optimization method is used to optimize the model, as explained in the Methods. As summarized in Fig. 4, the use of multiple convolutional layers allows for the detection of low-level features that cannot be detected with a single filter. It also allows for down-sampling and collection of relevant activations from previous layers, to be classified by a fully connected layer. In Fig. 4a, we represent 'active' features using a greyscale representation of the time-series data. Here, 50 two-dimensional (2D) convolutions are performed across each channel, resulting in 100 outputs in total. An additional 100 2D convolutions are performed on the second convolutional layer, resulting in the outputs shown in Fig. 4b. A fully connected layer of 1,024 units is produced, followed by a fully connected output layer with 5-class softmax activation (Fig. 4c). The mean accuracy results from SVM and CNN models for time-domain and CSDA data are shown in Fig. 4d,e, respectively. Of the four SVM kernel types tested, the highest accuracy results were chosen (cubic kernel) to be displayed for all results. This serves to establish universal applicability for the acquisition of SSVEPs using only two-channel SKINTRONICS. The same subject-to-subject cross-validation scheme was used for all training models. The results show that the SVM models are able

to achieve high accuracies with frequency-domain features for all kernel types. However, the linear SVM failed to classify time-domain signals beyond trivial accuracies. Overall, the optimized two-layer CNN was superior in all situations, due to its inherent ability to extract low-level features through shared weights, and its ability to be trained to detect many features that SVM cannot. On the basis of this evidence, this system and classification model can be trained on a small group of individuals and used in universal SSVEP-based BMI applications. To further emphasize these offline results, a confusion matrix, representing the results from the shortest data window input ($w = 0.512$ s), is summarized in Fig. 4f, where the wireless scalp system achieves a high accuracy ($94.54 \pm 0.90\%$) for a corresponding ITR of 122.1 ± 3.53 bits per minute (Table 1). In comparison, real-time cue-guided SSVEP test data across all 6 subjects show an accuracy of $94.01 \pm 3.6\%$ (Fig. 4g). These results show a consistent level of accuracy even with real-time classification, which allows for precise control over different interface targets, including an electric wheelchair, a wireless mini-vehicle and a communication (presentation) tool.

In vivo demonstration of a wireless BMI with human subjects. In this work, we demonstrate the feasibility of the SKINTRONICS system for a portable, wireless BMI via SSVEPs from six human subjects (Fig. 5). For the experiments, the subjects were seated in front of the light-emitting diode (LED) stimulus set-up, about 0.8 m away from their head at eye level where all 4 stimuli are presented simultaneously (Fig. 5a). The subjects conducted five tasks, including a null task (eyes closed for alpha rhythms) and gazing at four different LED locations (Fig. 5b), while the SKINTRONICS system securely conforms to the back of the subject's neck (Fig. 5c). The EEG data are recorded, displayed and saved in real time, along with the corresponding classification outputs, on an Android-based mobile device (Fig. 5d). A set of representative EEG data from five classes appears in Fig. 5e. The subjects used these data to control three target machines, including a wireless electric wheelchair (Pronto, Invacare; Fig. 5f), a wireless mini-vehicle (Minidrone, Parrot; Fig. 5g) and presentation software (PowerPoint 2016, Microsoft; Fig. 5h). Overall, subjects were able to achieve highly accurate and precise real-time control of three target machines with $94.01 \pm 3.6\%$ accuracy at 0.512-s intervals and $96.24 \pm 3.4\%$ at 1.024-s intervals. Subjects with various hair types and conditions were selected to ensure the electrode's performance in various scenarios (details of the BMI control scheme are provided in the Methods). A real-time, in vivo demonstration of the aforementioned machine controls with the SKINTRONICS system is shown in Supplementary Videos 1–3.

Discussion

The collection of materials presented here reports that a fully portable, wireless, ergonomic SKINTRONICS system offers highly accurate, real-time monitoring of SSVEPs on the scalp for a BMI. The flexible electronic system integrates a highly conformal wireless circuit on the back of the neck, a skin-like membrane electrode on the mastoid and three flexible conductive electrodes on the occipital lobe. The extremely small form factor and associated portability of the low-power SKINTRONICS system makes it less prone to interference and movement artefacts. The adherence to the skin and mechanically compliant electrodes allow for reasonable flexion and movements without any significant artefacts added to the EEG signals. Provided with these advantages, locations of highest signal density may be targeted with fewer electrodes, producing high-resolution signals from the areas of highest signal density. The electrode configuration is designed to target a consistently high SSVEP SNR across all subjects. A custom optimized algorithm using a deep learning CNN provides real-time, highly accurate classification of SSVEPs and a highly efficient ITR with only two channels (122.1 ± 3.53 bits per minute; Table 1), enabling precise control of a wireless wheelchair, a motorized mini-car and presentation software. Although two other systems[30,44] show higher ITRs than the SKINTRONICS system, they used a full benchtop system with an EEG cap and 9-channel gel electrodes. In addition, unlike these systems, the SKINTRONICS system used only flickering stimuli without any synchronization technique for enhanced accuracy, which requires additional work in the system. To mitigate a possible risk of collision or accident, the electric wheelchair can use a risk prevention system that may incorporate infrared or other proximity sensors[45]. In addition, the wheelchair can be bound to a specific set of paths to prevent accidents arising from misclassification.

Overall, the collective result in this work is significant owing to the decreased number of channels used when compared to other systems and because the device is also fully integrated for comfort and a low profile. Owing to the decreased number of channels, correlation-based analyses such as CCA and task-related component analysis could not be used. This control demonstrated by healthy subjects may easily be learned by subjects with weak or non-existent motor control (locked-in syndrome), requiring only movement of the eyes and closure of the eyelids. Using the combination of high-quality signals from two channels and an optimum classification method, we can achieve a high accuracy with limited information, demonstrating the possibility of a universal BMI. Furthermore, the EEG may be reconfigured to monitor motor evoked potentials[46] or motor imagination[47] for motor-impaired subjects, which will be further studied as a future work on therapeutic applications. For these applications, different electrodes will be used that are optimized for the required electrode locations and target signal characteristics. Furthermore, more randomization in performance comparison between multiple systems will be conducted along with different control targets.

Collectively, this paper reports fundamental strategies to design an ergonomic, portable EEG system for a broad range of assistive devices, smart-home systems and neuro-gaming interfaces. Future study would focus on investigation of fully elastomeric, wireless self-adhesive electrodes that can be mounted on the hairy scalp without any support from headgear, along with further miniaturization of the electronics to incorporate more electrodes for use with other studies.

Methods

Topographical mapping of SSVEP EEG data. The detailed methods for this process are recorded in Supplementary Section 1 and Supplementary Fig. 1. The representative sample of a topographical scalp captures the largest signal weights on the O1, O2 and Oz channels (other EEG mapping data from six human subjects appear in Supplementary Fig. 1d). These results are consistent with other topographical maps in a prior work[9]. For a deep neural network analysis, data were sampled at 256 Hz and the reference was set at Oz for the best results. The optimal electrode location was determined by a CNN trained to classify signals from all 32-channels (details of the architecture are shown in Supplementary Table 1). The trained weights for each channel could then be extracted and plotted using a topographical mapping algorithm provided by open EEGLAB (open source software)[48]. Details of this method are explained in Supplementary Section 1. This multi-channel quantitative EEG study retrospectively verifies the two optimal electrode locations that were used in the two-channel EEG study.

Preparation of SKINTRONICS. The device preparation consisted of three stages. First, using microfabrication processes, the thin-film flexible circuit boards were constructed on a polydimethylsiloxane-coated four-inch silicon wafer and peeled-off for subsequent steps[49]. The details of this process are given in Supplementary Section 1. Second, the surface mount chip components were soldered onto exposed copper pads by reflow soldering using a solder paste (SMDLTLFP10T5, Chip Quik). Third, electrode integration and device encapsulation were conducted. For electrode integration, polydimethylsiloxane-insulated conductive film cables (HST-9805210, Elform) were used to connect the dry electrodes and the flexible device while using a small amount of silver paint (Fast Drying Silver Paint, Ted Pella) as the adhesive for cable attachment. The assembled circuit was fully encapsulated with a low-modulus elastomer (Ecoflex 00-30, Smooth-On, Inc.) both to protect the circuit components and to provide the necessary adhesiveness and compliance for application on skin. Before the fabrication, the circuit design was validated on a printed board to confirm the optimized layout with matching antenna circuitry

(Supplementary Fig. 2a), along with the optimized components for a protocol of 2.45 GHz Bluetooth Low Energy. The reflection coefficient (S_{11}), plotted in Supplementary Fig. 2b, has a local minimum at 2.449 GHz of −29.68 dB, which allows for excellent telemetry at reasonably large ranges. The details of the device fabrication and encapsulation processes appear in Supplementary Section 2 and a step-by-step illustration is shown in Supplementary Fig. 3.

Recording of SSVEPs. Flexible elastomeric electrodes (placed at O1, O2 and Oz) are connected to the SKINTRONICS system through flexible thin-film cables, which are routed under the headband and connected on the right side of the device. In addition, a skin-conformal, aerosol-jet-printed electrode with improved skin adhesion reduces motion artefacts and enhances skin–electrode contact impedance. This electrode acts as a driven bias; therefore, its ability to capture EEG signals is outside the scope of this paper and not tested. The SKINTRONICS wireless telemetry unit uses a Bluetooth Low Energy microcontroller (nRF52832, Nordic Semiconductor) due to its high throughput, low latency, low power draw and wireless range[39]. The BLE protocol supports wireless synchronization of multiple devices to support greater numbers of channels[50]. Considering each SKINTRONICS system can support up to eight channels, more devices can be synchronized for measuring multi-EEG signals at different locations. For EEG recording, a front-end integrated circuit (ADS1299, Texas Instruments) was used, which is a low-noise 24-bit analog-to-digital converter with a built-in bias drive, while supporting up to eight differential-input channels (Supplementary Fig. 4a). The design also incorporates second-generation low-noise instrumentation amplifiers as the first gain stage (INA828, Texas Instruments). A schematic and block diagram of the connections for the external amplifiers are shown in Supplementary Fig. 4b, and the internal signal routing is listed in Supplementary Fig. 4c. The optimal configuration for the first gain stage was set to 100 V V^{-1} for use with dry electrodes, which provides an isolated low-noise, low-offset first gain stage. The internal programmable gain was set to 1 to minimize d.c. offset, harmonic distortion and amplifier saturation. To improve common-mode rejection, the driven ground electrode's bias amplifier was configured as an open loop. In this configuration, bias signals reached open-loop gain, which was the maximum possible gain achievable by the amplifier (Supplementary Fig. 4d). Parasitic capacitive effects[51] were limited through passive shielding with the elastomeric material on wiring and exposed electrode surfaces. A conventional bias electrode configuration is shown in Supplementary Fig. 4e.

Computational mechanics. Finite element analysis was conducted using commercial software (Abaqus FEA, Dassault Systemes) to determine mechanical behaviour under bending deformation at multiple locations. For the computational modelling, material properties (E, Young's modulus; ν, Poisson's ratio) of $E_{Cu} = 119$ GPa and $\nu_{Cu} = 0.34$ for copper and $E_{PI} = 2.5$ GPa and $\nu_{PI} = 0.34$ for polyimide were used[52,53].

Biaxial mechanical stretching. Biaxial stretching was used to test the stretchability of the skin-like flexible electrode used at the mastoid. Here, the electrode is placed in a custom-built biaxial stretcher (Supplementary Fig. 8), where opposite ends of a completed electrode are silver-pasted to copper wires that are connected to a digital multi-meter for resistance measurements. Biaxial stretching caused the resistance to increase as expected as the interconnects thinned, followed by a fracture at over 60% strain (Supplementary Fig. 9).

32-channel EEG recording. For determining precise electrode locations for placing a two-channel EEG device on the scalp, a deep learning-based topographic mapping procedure is used. A 32-channel EEG system (ActiveTwo System, Biosemi) was used to acquire data from subjects with active Ag/AgCl electrodes interfaced with the scalp through conductive water-based gel (Saline Base Signa Gel, Parker Laboratories). Impedances between measurement and ground electrodes were maintained below 10 kΩ during testing. The study involved 8 volunteers aged 18 to 40 and the study was conducted by following the approved Institutional Review Board protocol (no. H17212) at Georgia Institute of Technology. Before the in vivo study, all subjects agreed to the study procedures and provided signed consent forms.

Two-channel EEG recording. Target skin and scalp locations are cleaned with isopropyl alcohol before skin preparation. Abrasive skin preparation gel (NuPrep, Weaver and Co.) was gently applied to each of the electrode locations with a cotton swab to prepare the skin for electrode placement. Excess gel is removed using a gauze pad and the locations are cleaned with alcohol wipes before electrodes are applied. For the single skin electrode location, adhesive tape is used to remove dead skin cells from the surface and alcohol wipes are used to clean and prepare the skin. Impedances between the hair mount electrodes to ground were maintained below 20 kΩ. Due to the use of the flexible contacts of the scalp-mounted dry electrode and the skin-like electrode on the mastoid, we maintained the skin–electrode contact impedance at a relatively low level.

Calculation of SNR. The SNR was calculated from a continuously recorded 10 s sample, using the computed periodogram with 2,048-point (8.192 s) overlapping windows for each of the four stimuli. Data for each subject were recorded consecutively on the same day, starting with the ActiveTwo system, followed by the BioRadio system, and finally the SKINTRONICS system. The recordings from all three devices were performed within 2 h. The set-up time for the ActiveTwo system was about half an hour for each subject, while the BioRadio and SKINTRONICS systems were easier to set up due to the use of fewer electrodes (about 15 min to set up for each subject). The set-up time includes the skin preparation time and checking the electrode impedance before starting EEG recording. The time required to record all of the training and test data was about 13.5 min, for each system, with each individual trial being 75 s, with a minute break in between each of the 6 trials.

Calculation of ITR. SSVEP BCI systems are generally assessed on the basis of ITR, measured in bits per minute and their classification accuracy[54]. ITR is calculated as follows:

$$\mathrm{ITR} = \left(\log_2 N + A\log_2 A + (1-A)\log_2\left(\frac{1-A}{N-1}\right)\right) \times \left(\frac{60}{w}\right)\frac{\mathrm{bits}}{\mathrm{min}}$$

where N is the number of targets, A is the accuracy and w is the combined size of the classified windows in seconds and the gaze shift time[55]. For each instruction relayed through the interface, the incoming EEG data were evaluated three times, every 64 ms. Actions are taken if three consecutive windows are consistent, providing an additional layer of protection to prevent incorrect commands from being transmitted to targets. Using this method, the 4-class classification using CCA results in an ITR of 77.63 ± 5.32 bits per minute, with window length, $w = 0.94$ s, adjusted for gaze-shifting (+300 ms) and confusion protection (+128 ms). For testing the classification performance, a total of 30 individual stimuli were presented, for a total of 0.704 s, which allowed for classification of three consecutive 0.512 ms samples. This was used as a safety mechanism for the control interface, where action would be taken only with a majority decision (two or more classes match). Combined with gaze-shift time, that brings the length of the window used up to 0.94 s (0.512 + 0.3 + 0.128 s). This same process was repeated for all of the different window lengths. As a result, for each subject there were 450 samples of test data per trial for each window length, 90 for each class.

Feature extraction. The analysis includes comparison of time-domain and frequency-domain data using identical windows from the initial source in the form of single-window periodogram analysis and Welch PSDA. A third, coherence-based method, CSDA, was also implemented due to its ability to analyse the coherence of multiple channels, allowing for more precise frequency decomposition versus single-channel PSDA. Time-domain signals were preprocessed using a third-order Butterworth high-pass filter with a cutoff frequency of 4 Hz to remove d.c. offset and baseline drift. Owing to the high quality of the source signals, no other digital filtration was found to significantly improve the classification. These feature extraction methods are used to compare the learned feature-extraction capability of CNNs versus manual feature extraction with SVMs using various kernel functions (linear, quadratic, cubic and Gaussian).

Cross-validation of classification algorithms. For SVM and CNN classification, five subjects' training data were used to train the model and the remaining subject's data were used for evaluation. For the CNN, the training involved feeding a training batch of 256 and a test batch of 100 samples in each iteration. Following 3,000 training iterations (approximately 57 epochs), or, if no validation improvement occurs after 150 training steps, the training terminates. The test sets are subsequently evaluated for accuracy.

Experimental classes. We measure SSVEPs at four frequencies (11.1, 12.5, 15.2 and 16.7 Hz) and alpha rhythms to test the robustness of a system to specifically decode SSVEPs. We use alpha rhythms as the null class (no target interface action), intended for the user to relax their eyes in case of fatigue. Owing to the overlapping frequency ranges between alpha rhythms (8–12 Hz) and the intended SSVEP classes[56], the decoding process becomes more complex and error-prone for conventional machine learning techniques. Therefore, SSVEP frequencies below 11.1 Hz were not used due to frequency overlap with alpha rhythms. It was shown that short bursts of alpha rhythms could cause false positive results in these ranges[57]. The converse case is also a concern, where intentional alpha rhythms (subject has eyes closed) are incorrectly interpreted as SSVEPs within the alpha frequency band. Despite many prior works showing SSVEP-based systems within the alpha rhythm range, there has been limited study regarding confusion between SSVEP and alpha rhythm classification. Frequencies above 16.7 Hz were considered (18.5 and 20 Hz) in a 7-class SSVEP system and the average classification accuracy across all subjects is summarized in Supplementary Fig. 10. However, these frequencies were not included in the final system as they were considered extraneous, and some subjects had trouble focusing on these higher-frequency stimuli. The stimulus for this application included four green LEDs arranged on a 3D-printed hollow ring fixture. A microcontroller (nRF51, Nordic Semiconductor) controls the timings of the LEDs using a real-time operating system (FreeRTOS,

open-source software) to ensure correct timings. The timings to toggle each LED were set as 45 ms, 40 ms, 33 ms and 30 ms, corresponding to 11.1 Hz, 12.5 Hz, 15.2 Hz and 16.7 Hz, respectively.

Preparation of training and test data. For all experiments, a 250 Hz sampling rate was used with the SKINTRONICS system. The procedure for gathering training data involved a continuous EEG recording of 15 s for each class, separated by auditory cues. The classes were recorded in order of alpha rhythms, for the first 15 s, followed by 15 s of gazing at four different LED stimuli. Here, each recording where all five classes are performed constitutes a single trial. This trial was performed six times for each subject. Note that the experimental method for gathering training data is not the same as the experimental testing method. The experimental results showed that training from a continuous stimulus was significantly more effective than a fast (<1 s) cue-guided task. This may be because the relevant SSVEP features required for training are most optimal during these longer sessions of looking at the stimulus. To train the SVM and CNN models, the training data were sub-divided into window sizes of 128, 192, 256, 384 and 512 data points (corresponding to 0.512, 0.768, 1.024, 1.536 and 2.048 s data windows) to gauge changes in accuracy over different window sizes. The recording procedure for training and test data allowed for an additional 0.3 s for gaze-shifting between stimuli. From the training set, there were 2,700 samples from each subject used, 450 samples from each of the 6 recordings. Therefore, for 5 subjects, a single training epoch consisted of training on 13,500 samples.

Grid-search optimization of CNNs. In all CNN models, the filters and other trained variables were optimized using an optimization algorithm with a constant learning rate (Adam, learning rate = 0.001, $\beta_1 = 0.9$, $\beta_2 = 0.999$)[58], and the error was calculated using the cross-entropy loss function. The input to the network is a 2D array of (n, 2), where n is the number of data points for a window sampled at 250 Hz (for example, $n = 128$, for a window length of 0.512 s), and the 2 represents the two channels. This work optimizes the baseline CNN (architecture in Supplementary Table 2) through two stages of improvements, adjusting components and hyperparameters on a single layer. A grid-search approach was used because training for such a small dataset could be completed in a few minutes on consumer hardware, and it was reasonably efficient to find an optimal solution. First, the optimum parameters are determined for a CNN with one convolutional layer and one fully connected layer before the output layer. This model is then expanded to multiple layers, as needed, to further improve accuracy. Details of the optimization procedure via grid-search appear in Supplementary Section 8 and are illustrated in Supplementary Figs. 13–16 and Supplementary Tables 3–8. The optimized CNN for time-domain (2-CNN-TD) and CSDA (2-CNN-CSDA) data can be found in Supplementary Tables 9 and 10, respectively. The optimization of the CNN results in enhanced classification accuracy from six subjects (Supplementary Tables 11–14). To demonstrate the device performance, the same optimized CNN procedure was performed on data from two commercial systems (BioRadio and ActiveTwo) and is summarized in Supplementary Tables 15 and 16 and Supplementary Fig. 17.

BMI control scheme. An Android-based operating system was selected to demonstrate the functionality and feasibility of a fully portable, wireless BMI. The SSVEP data transmitted from the SKINTRONICS system with short electrode cables (Supplementary Table 17) was received by a Bluetooth-enabled smartphone (Samsung Galaxy S7). The data were preprocessed and fed into the trained CNN for classification on the smartphone. The output of the classification was used to wirelessly control the interface target. For the electric wheelchair and wireless vehicle, the methods of control are the same as they are both two-wheel-drive vehicles. When the subject has their eyes closed, the vehicle does not move, and it begins to move only once the SSVEP is classified by the central processing device. The top LED (11.1 Hz) is used to program the forward motion of the wheelchair and the vehicle. The right-facing 15.2 Hz LED results in an anticlockwise rotation, while the left-facing 12.5 Hz results in a clockwise rotation. The final 16.7 Hz LED operates the reverse functionality. For the presentation control interface, the top LED initiates the start of the presentation, the right LED proceeds forward through the slides and the left LED reverts to the previous slide. Last, the bottom LED terminates the presentation. Note that six subjects participated in the BMI control study (their hair information and associated EEG SNR are shown in Supplementary Table 18). Overall, this BMI control demonstration with the wireless, portable SKINTRONICS system shows the potential for other neuro-interface applications, as the controls can be easily reassigned to any target with equivalent or fewer targets. Furthermore, this method can be scaled up to include a greater number of classes, which was previously not possible due to a lack of signal quality.

Reporting Summary. Further information on research design is available in the Nature Research Reporting Summary linked to this article.

Data availability

The EEG data recorded for this work are available on the Open Science Framework (https://osf.io/nyfa7/).

Code availability

The code for the CNN models are available on GitLab (https://gitlab.com/musasmahmood/ssvep-cnn-demo).

Received: 20 March 2019; Accepted: 25 July 2019;
Published online: 11 September 2019

References

1. Garcia, J. O., Srinivasan, R. & Serences, J. T. Near-real-time feature-selective modulations in human cortex. *Curr. Biol.* **23**, 515–522 (2013).
2. Zhu, D., Bieger, J., Garcia Molina, G. & Aarts, R. M. A survey of stimulation methods used in SSVEP-based BCIs. *Comput. Intell. Neurosci.* **2010**, 702357 (2010).
3. Luo, A. & Sullivan, T. J. A user-friendly SSVEP-based brain-computer interface using a time-domain classifier. *J. Neural Eng.* **7**, 26010 (2010).
4. Stamps, K. & Hamam, Y. Towards inexpensive BCI control for wheelchair navigation in the enabled environment - a hardware survey. *Lect. Notes Artif. Int.* **6334**, 336–345 (2010).
5. Guger, C. et al. How many people could use an SSVEP BCI? *Front. Neurosci.* **6**, 169 (2012).
6. Ramos-Murguialday, A. et al. Brain–machine interface in chronic stroke rehabilitation: a controlled study. *Ann. Neurol.* **74**, 100–108 (2013).
7. Soekadar, S. R., Birbaumer, N., Slutzky, M. W. & Cohen, L. G. Brain–machine interfaces in neurorehabilitation of stroke. *Neurobiol. Dis.* **83**, 172–179 (2015).
8. Nicolas-Alonso, L. F. & Gomez-Gil, J. Brain computer interfaces, a review. *Sensors* **12**, 1211–1279 (2012).
9. Bin, G., Lin, Z., Gao, X., Hong, B. & Gao, S. The SSVEP topographic scalp maps by canonical correlation analysis. In *Conf. Proc. IEEE Eng. Med. Biol. Soc.* 3759–3762 (IEEE, 2008).
10. Wang, Y., Wang, R., Gao, X., Hong, B. & Gao, S. A practical VEP-based brain–computer interface. *IEEE Trans. Neural Syst. Rehabil. Eng.* **14**, 234–239 (2006).
11. Wang, Y., Gao, X., Hong, B., Jia, C. & Gao, S. Brain–computer interfaces based on visual evoked potentials. *IEEE Eng. Med. Biol. Mag.* **27**, 64–71 (2008).
12. Kelly, S. P., Lalor, E. C., Reilly, R. B. & Foxe, J. J. Visual spatial attention tracking using high-density SSVEP data for independent brain–computer communication. *IEEE Trans. Neural Syst. Rehabil. Eng.* **13**, 172–178 (2005).
13. Herrmann, C. S. Human EEG responses to 1–100 Hz flicker: resonance phenomena in visual cortex and their potential correlation to cognitive phenomena. *Exp. Brain Res.* **137**, 346–353 (2001).
14. Wang, Y., Wang, Y. T. & Jung, T. P. Visual stimulus design for high-rate SSVEP BCI. *Electron. Lett.* **46**, 1057–1058 (2010).
15. Norton, J. J. S. et al. Soft, curved electrode systems capable of integration on the auricle as a persistent brain–computer interface. *Proc. Natl Acad. Sci. USA* **112**, 3920–3925 (2015).
16. Beverina, F., Palmas, G., Silvoni, S., Piccione, F. & Giove, S. User adaptive BCIs: SSVEP and P300 based interfaces. *PsychNology J.* **1**, 331–354 (2003).
17. Kronegg, J., Voloshynovskiy, S. & Pun, T. Analysis of bit-rate definitions for brain–computer interfaces. In *HCI '05: Proc. 2005 International Conference on Human–Computer Interaction* 40–46 (HCI International, 2005).
18. Lin, Z., Zhang, C., Wu, W. & Gao, X. Frequency recognition based on canonical correlation analysis for SSVEP-based BCIs. *IEEE Trans. Biomed. Eng.* **54**, 1172–1176 (2007).
19. Martinez, P., Bakardjian, H. & Cichocki, A. Fully online multicommand brain–computer interface with visual neurofeedback using SSVEP paradigm. *Comput. Intell Neurosci.* **2007**, 94561 (2007).
20. Bin, G., Gao, X., Yan, Z., Hong, B. & Gao, S. An online multi-channel SSVEP-based brain–computer interface using a canonical correlation analysis method. *J. Neural Eng.* **6**, 046002 (2009).
21. Wang, Y. T., Wang, Y., Cheng, C. K. & Jung, T. P. Measuring steady-state visual evoked potentials from non-hair-bearing areas. In *Conf. Proc. IEEE Eng. Med. Biol. Soc.* 1806–1809 (IEEE, 2012).
22. Cecotti, H. A time–frequency convolutional neural network for the offline classification of steady-state visual evoked potential responses. *Pattern Recognit. Lett.* **32**, 1145–1153 (2011).
23. McAdams, E. T., Jossinet, J., Lackermeier, A. & Risacher, F. Factors affecting electrode–gel–skin interface impedance in electrical impedance tomography. *Med. Biol. Eng. Comput.* **34**, 397–408 (1996).
24. Searle, A. & Kirkup, L. A direct comparison of wet, dry and insulating bioelectric recording electrodes. *Physiol. Meas.* **21**, 271–283 (2000).
25. Li, G., Wang, S. & Duan, Y. Y. Towards gel-free electrodes: a systematic study of electrode–skin impedance. *Sens. Actuators B* **241**, 1244–1255 (2017).
26. Lin, C. T. et al. Review of wireless and wearable electroencephalogram systems and brain-computer interfaces - a mini-review. *Gerontology* **56**, 112–119 (2010).
27. Salvo, P. et al. A 3D printed dry electrode for ECG/EEG recording. *Sens. Actuators A* **174**, 96–102 (2012).

28. Stauffer, F. et al. Skin conformal polymer electrodes for clinical ECG and EEG recordings. *Adv. Healthc. Mater.* **7**, e1700994 (2018).
29. Tallgren, P., Vanhatalo, S., Kaila, K. & Voipio, J. Evaluation of commercially available electrodes and gels for recording of slow EEG potentials. *Clin. Neurophysiol.* **116**, 799–806 (2005).
30. Nakanishi, M. et al. Enhancing detection of SSVEPs for a high-speed brain speller using task-related component analysis. *IEEE Trans. Biomed. Eng.* **65**, 104–112 (2018).
31. Kwak, N. S., Muller, K. R. & Lee, S. W. A convolutional neural network for steady state visual evoked potential classification under ambulatory environment. *PLoS ONE* **12**, e0172578 (2017).
32. Dufort y Alvarez, G. et al. Wireless EEG system achieving high throughput and reduced energy consumption through lossless and near-lossless compression. *IEEE Trans. Biomed. Circuits Syst.* **12**, 231–241 (2018).
33. Lin, C.-T., Chiu, C.-Y., Singh, A. K., King, J.-T. & Wang, Y.-K. A wireless multifunctional SSVEP-based brain computer interface assistive system. *IEEE Trans. Cogn. Dev. Syst.* 1 (IEEE, 2018).
34. Schlogl, A., Keinrath, C., Scherer, R. & Furtscheller, P. Information transfer of an EEG-based brain computer interface. In *Proc. First International IEEE EMBS Conference on Neural Engineering* 641–644 (IEEE, 2003).
35. Xu, J. & Zhong, B. Review on portable EEG technology in educational research. *Comput. Hum. Behav.* **81**, 340–349 (2018).
36. Shi, M. et al. Towards portable SSVEP-based brain-computer interface using Emotiv EPOC and mobile phone. In *Proc. Tenth International Conference on Advanced Computational Intelligence* 249–253 (IEEE, 2018).
37. Chen, X., Zhao, B., Wang, Y., Xu, S. & Gao, X. Control of a 7-DOF robotic arm system with an SSVEP-based BCI. *Int. J. Neural Syst.* **28**, 1850018 (2018).
38. Mishra, S. et al. Soft, conformal bioelectronics for a wireless human–wheelchair interface. *Biosens. Bioelectron.* **91**, 796–803 (2017).
39. Lee, Y. et al. Wireless, intraoral hybrid electronics for real-time quantification of sodium intake toward hypertension management. *Proc. Natl Acad. Sci. USA* **115**, 5377–5382 (2018).
40. Chi, Y. M. et al. A practical mobile dry EEG system for human computer interfaces. In *Proc. International Conference on Augmented Cognition* 649–655 (Springer, 2013).
41. Mullen, T. R. et al. Real-time neuroimaging and cognitive monitoring using wearable dry EEG. *IEEE Trans. Biomed. Eng.* **62**, 2553–2567 (2015).
42. Lee, Y. et al. Soft electronics enabled ergonomic human–computer interaction for swallowing training. *Sci. Rep.* **7**, 46697 (2017).
43. Krizhevsky, A., Sutskever, I. & Hinton, G. E. Imagenet classification with deep convolutional neural networks. *Adv. Neural Inf. Process. Syst.* **1**, 1097–1105 (2012).
44. Chen, X. et al. High-speed spelling with a noninvasive brain–computer interface. *Proc. Natl Acad. Sci. USA* **112**, E6058–E6067 (2015).
45. Ji, Y., Hwang, J. & Kim, E. Y. An intelligent wheelchair using situation awareness and obstacle detection. *Procedia* **97**, 620–628 (2013).
46. Ma, T. et al. The hybrid BCI system for movement control by combining motor imagery and moving onset visual evoked potential. *J. Neural Eng.* **14**, 026015 (2017).
47. Pfurtscheller, G. & Neuper, C. Motor imagery and direct brain–computer communication. *Proc. IEEE* **89**, 1123–1134 (2001).
48. Delorme, A. & Makeig, S. EEGLAB: an open source toolbox for analysis of single-trial EEG dynamics including independent component analysis. *J. Neurosci. Methods* **134**, 9–21 (2004).
49. Kim, Y. S. et al. Scalable manufacturing of solderable and stretchable physiologic sensing systems. *Adv. Mater.* **29**, 1701312 (2017).
50. Bideaux, A., Zimmermann, B., Hey, S. & Stork, W. Synchronization in wireless biomedical-sensor networks with Bluetooth Low Energy. *Curr. Dir. Biomed. Eng.* **1**, 73–76 (2015).
51. Mastinu, E., Ortiz-Catalan, M. & Hakansson, B. Analog front-ends comparison in the way of a portable, low-power and low-cost EMG controller based on pattern recognition. In *Conf. Proc. IEEE Eng. Med. Biol. Soc.* 2111–2114 (IEEE, 2015).
52. Zhang, Y., Zhou, G., Jin, J., Wang, X. & Cichocki, A. Frequency recognition in SSVEP-based BCI using multiset canonical correlation analysis. *Int. J. Neural Syst.* **24**, 1450013 (2014).
53. Xu, R. et al. Fabric-based stretchable electronics with mechanically optimized designs and prestrained composite substrates. *Extreme Mech. Lett.* **1**, 120–126 (2014).
54. Obermaier, B., Neuper, C., Guger, C. & Pfurtscheller, G. Information transfer rate in a five-classes brain–computer interface. *IEEE Trans. Neural Syst. Rehabil. Eng.* **9**, 283–288 (2001).
55. Shannon, C. E. & Weaver, W. *The Mathematical Theory of Information* (Univ. Illinois Press, 1949).
56. Goldman, R. I., Stern, J. M., Engel, J.Jr & Cohen, M. S. Simultaneous EEG and fMRI of the alpha rhythm. *Neuroreport* **13**, 2487–2492 (2002).
57. Wang, Y., Wang, R., Gao, X. & Gao, S. Brain-computer interface based on the high-frequency steady-state visual evoked potential. In *Proc. First International Conference on Neural Interface and Control* 37–39 (IEEE, 2005).
58. Kingma, D. P. & Ba, J. Adam: a method for stochastic optimization. Preprint at https://arxiv.org/abs/1412.6980 (2014).
59. Bevilacqua, V. et al. A novel BCI-SSVEP based approach for control of walking in virtual environment using a convolutional neural network. In *Proc. IEEE International Joint Conference on Neural Networks (IJCNN)* 4121–4128 (IEEE, 2014).
60. Volosyak, I. SSVEP-based Bremen–BCI interface—boosting information transfer rates. *J. Neural Eng.* **8**, 036020 (2011).

Acknowledgements

W.-H.Y. acknowledges a grant from the Fundamental Research Program (project PNK5061) of Korea Institute of Materials Science, funding by the Nano-Material Technology Development Program through the National Research Foundation of Korea (NRF) funded by the Ministry of Science, ICT and Future Planning (no. 2016M3A7B4900044), and support from the Institute for Electronics and Nanotechnology, a member of the National Nanotechnology Coordinated Infrastructure, which is supported by the National Science Foundation (grant ECCS-1542174).

Author contributions

M.M. and W.-H.Y. designed the research project; M.M., D.M., Y.-S.K., Y.L., R.H., A.D., S.M., C.S.A. and W.-H.Y. performed research; M.M., D.M., A.D., C.S.A. and W.-H.Y. analysed data; and M.M., D.M., C.S.A. and W.-H.Y. wrote the paper.

Competing interests

W.-H.Y. and M.M. are the inventors on a pending US patent application.

Additional information

Supplementary information is available for this paper at https://doi.org/10.1038/s42256-019-0091-7.

Reprints and permissions information is available at www.nature.com/reprints.

Correspondence and requests for materials should be addressed to W.-H.Y.

Publisher's note: Springer Nature remains neutral with regard to jurisdictional claims in published maps and institutional affiliations.

nature research

Corresponding author(s): Woon-Hong Yeo

Last updated by author(s): 04/03/2019

Reporting Summary

Nature Research wishes to improve the reproducibility of the work that we publish. This form provides structure for consistency and transparency in reporting. For further information on Nature Research policies, see Authors & Referees and the Editorial Policy Checklist.

Statistics

For all statistical analyses, confirm that the following items are present in the figure legend, table legend, main text, or Methods section.

n/a	Confirmed	
☐	☒	The exact sample size (*n*) for each experimental group/condition, given as a discrete number and unit of measurement
☒	☐	A statement on whether measurements were taken from distinct samples or whether the same sample was measured repeatedly
☒	☐	The statistical test(s) used AND whether they are one- or two-sided *Only common tests should be described solely by name; describe more complex techniques in the Methods section.*
☒	☐	A description of all covariates tested
☒	☐	A description of any assumptions or corrections, such as tests of normality and adjustment for multiple comparisons
☒	☐	A full description of the statistical parameters including central tendency (e.g. means) or other basic estimates (e.g. regression coefficient) AND variation (e.g. standard deviation) or associated estimates of uncertainty (e.g. confidence intervals)
☒	☐	For null hypothesis testing, the test statistic (e.g. *F*, *t*, *r*) with confidence intervals, effect sizes, degrees of freedom and *P* value noted *Give P values as exact values whenever suitable.*
☒	☐	For Bayesian analysis, information on the choice of priors and Markov chain Monte Carlo settings
☒	☐	For hierarchical and complex designs, identification of the appropriate level for tests and full reporting of outcomes
☒	☐	Estimates of effect sizes (e.g. Cohen's *d*, Pearson's *r*), indicating how they were calculated

Our web collection on statistics for biologists contains articles on many of the points above.

Software and code

Policy information about availability of computer code

Data collection	Custom code used for data collection includes Android application code for the monitoring software, and the firmware used in the SKINTRONICS device microcontroller. The android software recorded and labeled the data at the same time.
Data analysis	MATLAB was used to preprocess and separate the data. Keras and Tensorflow were used to create the CNN models for data classification.

For manuscripts utilizing custom algorithms or software that are central to the research but not yet described in published literature, software must be made available to editors/reviewers. We strongly encourage code deposition in a community repository (e.g. GitHub). See the Nature Research guidelines for submitting code & software for further information.

Data

Policy information about availability of data

All manuscripts must include a data availability statement. This statement should provide the following information, where applicable:

- Accession codes, unique identifiers, or web links for publicly available datasets
- A list of figures that have associated raw data
- A description of any restrictions on data availability

The data that support the findings of this study are available from the corresponding author upon reasonable request.

Field-specific reporting

Please select the one below that is the best fit for your research. If you are not sure, read the appropriate sections before making your selection.

☒ Life sciences ☐ Behavioural & social sciences ☐ Ecological, evolutionary & environmental sciences

Life sciences study design

All studies must disclose on these points even when the disclosure is negative.

Sample size	This is a pilot study, therefore no sample size calculation was performed.
Data exclusions	No data were excluded
Replication	To verify the brain-machine interface worked across subject, we used cross-validation across all 6 subjects involved, with the results suggesting that this study is easily repeatable.
Randomization	N/A. There were no experimental groups. All subjects experienced the same tests.
Blinding	N/A. There were no experimental groups. All subjects experienced the same tests.

Reporting for specific materials, systems and methods

We require information from authors about some types of materials, experimental systems and methods used in many studies. Here, indicate whether each material, system or method listed is relevant to your study. If you are not sure if a list item applies to your research, read the appropriate section before selecting a response.

Materials & experimental systems

n/a	Involved in the study
☒	☐ Antibodies
☒	☐ Eukaryotic cell lines
☒	☐ Palaeontology
☒	☐ Animals and other organisms
☐	☒ Human research participants
☒	☐ Clinical data

Methods

n/a	Involved in the study
☒	☐ ChIP-seq
☒	☐ Flow cytometry
☒	☐ MRI-based neuroimaging

Human research participants

Policy information about studies involving human research participants

Population characteristics	S1. Male, Age 24, Caucasian, no relevant diagnosis S2. Male, Age 22, East-Asian, no relevant diagnosis S3. Male, Age 19, Caucasian, no relevant diagnosis S4. Male, Age 21, Caucasian, no relevant diagnosis S5. Male, Age 30, Caucasian, no relevant diagnosis S6. Male, Age 22, East-Asian, no relevant diagnosis S7. Male, Age 40, East-Asian, no relevant diagnosis
Recruitment	Subjects were recruited from Georgia Tech based on the approved protocol.
Ethics oversight	The study was conducted by following the approved IRB protocol (# H17212) at Georgia Institute of Technology

Note that full information on the approval of the study protocol must also be provided in the manuscript.